


## Table-top ion-trap experiment on the stability of intense short bunches in linear hadron accelerators

M. Kuroda, A. Kasagaki, H. Okamoto<sup>✉,\*</sup> and K. Ito<sup>✉</sup>

*Graduate School of Advanced Science and Engineering, Hiroshima University,  
1-3-1 Kagamiyama, Higashi-Hiroshima 739-8530, Japan*

 (Received 21 January 2024; accepted 29 April 2024; published 21 May 2024)

The novel experimental system “S-POD” (Simulator of Particle Orbit Dynamics) is employed to explore the stability of short hadron bunches in high-intensity linacs. In a previous study with the S-POD [M. Goto et al., *Phys. Rev. Accel. Beams* **25**, 054201 (2022)], a static potential was used to focus the bunch in the longitudinal direction. We here make a step forward to include the possibility of pure synchrotron resonance, introducing periodic modulation to the longitudinal potential well. The modulation period was taken a half of the transverse alternating-gradient focusing period, which reflects the most typical lattice condition of a drift-tube linac. Detailed stability maps are constructed to reveal dangerous parameter regions where serious beam loss may occur due to resonance. We reconfirm the existence of various betatron and synchrotron resonance stop bands whose widths and locations change in tune space depending on the bunch intensity. It turns out that the periodicity of the longitudinal focusing potential brings about no pronounced effect on the resonance feature; the result is very similar to what we obtained in the previous study with a static longitudinal potential. As long as the lattice periodicity mentioned above is maintained, no serious noncoupling synchrotron resonance appears even with a high synchrotron phase advance above  $90^\circ$  per unit alternating-gradient cell. Severe envelope instability may, however, be excited in the longitudinal direction if the axial focusing force includes error components that affect the original lattice periodicity. The experimental observations can be explained with the *stop-band diagram* free from the concept of incoherent tune spread.

DOI: [10.1103/PhysRevAccelBeams.27.054201](https://doi.org/10.1103/PhysRevAccelBeams.27.054201)

### I. INTRODUCTION

In high-intensity hadron accelerators, natural Coulomb interaction among accelerated particles plays a crucial role in beam stability [1]. Space-charge-induced effects are generally more severe at a lower beam energy, which means that extra attention is required for the basic design of an injector linac. In fact, they set an upper limit on the allowable phase advance of betatron oscillation; the bare phase advance is supposed to be chosen below  $90^\circ$  per unit alternating-gradient (AG) focusing cell so that we can avoid serious beam loss due to the excitation of the second-order collective resonance driven by the Coulomb self-field potential [2,3].

A systematic study of space-charge effects is not so easy in practice. The flexibility and controllability of operating tunes and other fundamental beam-dynamics quantities are

quite limited in most accelerators, which forces one to give up a wide-range survey of parameter space. Self-consistent theoretical investigation is also very tough as the beam consists of a huge number of particles interacting each other. To overcome these difficulties in conventional approaches, we constructed the novel experimental apparatus named “S-POD” (Simulator of Particle Orbit Dynamics) that allows for detailed exploration of various space-charge issues in a local tabletop environment [4]. A similar Paul-trap system “IBEX” (Intense Beam EXperiment) is in operation at the Rutherford Appleton Laboratory in the United Kingdom to support theoretical studies of next-generation high-intensity accelerators [5].

An ion cloud provided by the S-POD obeys the equations of motion almost identical to those for a relativistic beam travelling in an AG focusing channel [6,7]. What occurs in the former dynamical system, therefore, occurs in the latter and vice versa, so we can elucidate the nature of intense hadron beams experimentally without relying on large-scale machines.

In past S-POD experiments, we mostly employed axially long ion clouds of sausage-like configurations, bearing a long bunch or coasting beam in mind. The linear Paul trap (LPT) dedicated to the present study is designed to produce

\*Corresponding author: [okamoto@sci.hiroshima-u.ac.jp](mailto:okamoto@sci.hiroshima-u.ac.jp)

*Published by the American Physical Society under the terms of the Creative Commons Attribution 4.0 International license. Further distribution of this work must maintain attribution to the author(s) and the published article's title, journal citation, and DOI.*

an ellipsoidal ion cloud whose aspect ratio is around unity [8]. Such a short bunch is typical in injector linacs. Comprehensive experimental data on a short-bunch stability were recently acquired under a simplified lattice condition, i.e., with a time-independent potential well along the LPT axis [9]. We here make the axial ion confinement force periodic and see if any essential difference from the simple static confinement case arises.

The paper is organized as follows. In Sec. II, we start with a brief description of the S-POD system and experimental procedure. Before proceeding to experimental observations, the resonance theory developed by the authors' group is briefly reviewed in Sec. III, followed by results of self-consistent multiparticle simulations in Sec. IV. Section V is devoted to a summary of S-POD experiments that reveal a short-bunch stability in the low-density and high-density regimes. Concluding remarks are finally made in Sec. VI.

## II. S-POD

The core of the S-POD apparatus is a compact LPT sitting in a vacuum chamber, where the base pressure is kept below  $10^{-8}$  Pa [10]. As illustrated in Fig. 1, the ion trap consists of three independent quadrupole sections 0.5 mm apart from each other. The minimum distance from the LPT axis to the electrode surfaces is  $r_0 = 5$  mm. Ions are stored in the central section, where an axial potential well is created by dc or ac voltages  $V_{\parallel}$  added to the quadrupole sections on both sides. A radio-frequency (rf) quadrupole field is excited in all three sections for transverse ion confinement. The frequency of the quadrupole field is fixed at 1 MHz.

What ion species we use for the S-POD experiment is unessential for the physics of interest to us here; the mass and charge state of the ions are just a part of scaling parameters to determine some important beam-dynamics quantities, such as the betatron and synchrotron phase advances and tune depressions. Among several possible choices, we picked  $^{40}\text{Ar}^+$  that can readily be produced from neutral Ar gas through the electron bombardment process.

The length of the central quadrupole rods (8.9 mm) has been optimized to make the axial ion confinement potential

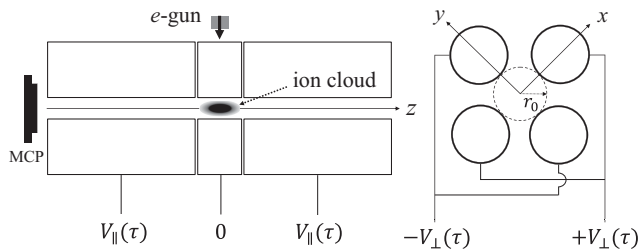


FIG. 1. Schematic layout of the LPT electrodes and other components.

nearly parabolic. An approximate Hamiltonian describing the motion of an ion cloud in the LPT is then given by

$$H = \frac{p_x^2 + p_y^2 + p_z^2}{2} + \frac{K_{\perp}(\tau)}{2}(x^2 - y^2) + \frac{K_{\parallel}(\tau)}{2}\left(z^2 - \frac{x^2 + y^2}{2}\right) + I_q \phi_{sc}(x, y, z; \tau), \quad (1)$$

where  $K_{\perp}(\tau)$  is proportional to the rf quadrupole voltage  $V_{\perp}$  for transverse ion confinement while  $K_{\parallel}(\tau)$  to the additional bias  $V_{\parallel}$  for axial ion confinement,  $I_q$  is a constant depending on the bunch intensity,  $\phi_{sc}$  represents the Coulomb self-field potential, and the independent variable is  $\tau = ct$  with  $c$  being the speed of light. Note that  $V_{\parallel}$  applied to the two end sections generates a transverse defocusing force, which corresponds to the effect known as *rf defocusing* in accelerating gaps [11]. This Hamiltonian is basically the same as that often assumed in past theoretical studies of space-charge effects in AG beam transport channels [1–3,8,11].

The most standard waveform for the transverse focusing function  $K_{\perp}(\tau)$  is the FODO type (Focus-Drift-Defocus-Drift) widely adopted in drift-tube linacs (DTLs). Our previous experimental and numerical studies have demonstrated that there is no significant difference in resonance features between the sinusoidal focusing and FODO lattice [12,13]. For the present experiment, therefore, we used the simple sinusoidal  $V_{\perp}$  oscillating at 1 MHz. Each FODO period includes two accelerating gaps if all drift tubes have a quadrupole magnet inside. Considering this fact, the waveform of the axial focusing function  $K_{\parallel}(\tau)$  was taken as sketched in Fig. 2.  $V_{\parallel}$  oscillating at 2 MHz must always be positive because the bunch receives only a focusing force axially at every gap (weak focusing). The synchrotron phase advance  $\sigma_{\parallel}$  per FODO cell is determined solely by  $V_{\parallel}$ , while the betatron phase advance  $\sigma_{\perp}$  depends on both  $V_{\perp}$  and  $V_{\parallel}$  as is evident from Eq. (1). In what follows, we assume for simplicity that the horizontal and vertical phase advances are both equal to  $\sigma_{\perp}$ .

The initial number of ions can be controlled by changing the electron beam current from the *e*-gun and/or the amount of neutral Ar gas introduced in the chamber. The ionization procedure typically lasts for about 1 s. We then shut down the *e*-gun, store  $\text{Ar}^+$  ions for a certain period at a certain operating point, and finally launch surviving ions from the trap toward the microchannel plate (MCP) detector by removing the axial potential barrier on the MCP side. This measurement cycle takes only several seconds, including the data transfer to a hard disk unit for saving. The whole experimental procedure is automated. After completion of a single measurement cycle, the operating betatron and synchrotron phase advances are changed to another target values automatically until the end of a stability survey over a wide area in  $\sigma_{\perp}$ - $\sigma_{\parallel}$  plane.

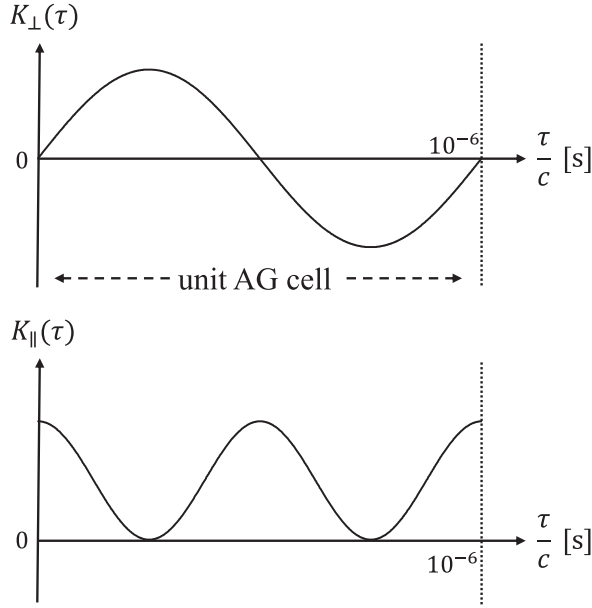


FIG. 2. Waveforms of the focusing functions  $K_{\perp}(\tau)$  and  $K_{\parallel}(\tau)$ .  $K_{\perp}(\tau)$  oscillates at 1 MHz while  $K_{\parallel}(\tau)$  at 2 MHz.

### III. RESONANCE CONDITIONS AND STOP-BAND DIAGRAM

The concept of *incoherent tune spread* or the so-called *necktie diagram* has been commonly used to explain resonance-induced particle losses observed especially in circular machines. Such a conventional notion, however, does not work very well as the motions of individual particles in the beam core are not independent but rather correlated through the Coulomb self-fields [1,2,14,15]. In fact, neither self-consistent numerical simulation results nor experimental observations with the S-POD can be understood on the basis of the incoherent picture [13,16–20]. The collective (coherent) nature of the beam core needs to be taken carefully into account to make reasonable predictions about the stability of space-charge-dominated beams.

A universal guideline applicable to both linear and circular accelerators was recently established to avoid low-order resonances at high space-charge density [21,22]. Dangerous operating tunes at which non-negligible beam loss may occur can be predicted with the *stop-band diagram* rather than the necktie. The new type of stability chart is based on the coherent betatron resonance condition first conjectured in Ref. [13] from the one-dimensional (1D) Vlasov theory in Ref. [23]. The proposed two-dimensional (2D) condition was soon generalized to treat coherent core resonances in bunched beams [24]. When the transverse betatron tunes are equal as assumed here, we expect core resonances of the  $m$ th order to be excited around the lines defined by

$$n_{\perp}\sigma_{\perp}[1 - C_m(1 - \eta_{\perp})] + n_{\parallel}\sigma_{\parallel}[1 - C_m(1 - \eta_{\parallel})] = n180^{\circ}, \quad (2)$$

where  $(n_{\perp}, n_{\parallel}, n)$  are integers, and  $C_m$  is a  $m$ -dependent constant.  $\eta_{\perp}$  and  $\eta_{\parallel}$  are the transverse and longitudinal root-mean-squared (rms) tune depressions evaluated from the three-dimensional (3D) rms envelope equations [25]. The rms tune depression is a measure of beam density in phase space, which ranges from 0 (high-density limit) to 1 (low-density limit).

The coherent tune-shift factor  $C_m$  is always positive but less than unity. It increases as the resonance order  $m$  becomes higher. According to the pioneering work by Sacherer [26],  $C_1 = 0$  (dipole mode),  $C_2 = 0.75$  (quadrupole mode),  $C_3 = 0.875$  (sextupole mode),  $C_4 = 0.922$  (octupole mode), etc., for a 1D sheet beam. Recent particle-in-cell (PIC) simulations for coasting beams have concluded the values of  $C_m$  roughly consistent with the Vlasov prediction [16], i.e.,  $C_2 \approx 0.7$ ,  $C_3 \approx 0.8$ , and  $C_4 \approx 0.9$ .

Experimental determination of the  $C_m$  factor is extremely difficult even with the S-POD and IBEX trap systems [27,28]. For this purpose, precise information is necessary as to how a coherent stop band of the  $m$ th order shifts depending on the bunch density. Such information is currently obtained from the simple ion-loss measurement, but in that case, we cannot distinguish whether the instability occurred collectively in the core or incoherently in the tail. The size of  $C_m$  is usually underestimated when we rely on ion-loss data [16].

Of particular note is the fact that the right-hand side of Eq. (2) is not an integer multiple of  $360^{\circ}$  as in standard resonance conditions but an integer multiple of  $180^{\circ}$ . This leads to a two-fold increase of the density of resonances in tune space. External driving fields originating from machine imperfections and correction magnets enhance coherent resonances of the same order but only with even  $n$  in Eq. (2), while the natural Coulomb self-field can drive all resonances regardless of the parity of  $n$ . The procedure for drawing a stop-band diagram based on the coherent picture is outlined in Ref. [21] (see also Ref. [22] for more information).

Each coherent instability band is accompanied by an incoherent resonance domain within which large-amplitude particles in the beam tail might become unstable almost independently. The order of the incoherent tail resonance driven by the space-charge potential is twice higher than that of the neighboring coherent instability. Space-charge-induced resonances of tail particles adjacent to the coherent core resonance band of Eq. (2) are activated under the condition [22]

$$2n_{\perp}(\sigma_{\perp} - \Delta\sigma_{\perp}) + 2n_{\parallel}(\sigma_{\parallel} - \Delta\sigma_{\parallel}) = n360^{\circ}, \quad (3)$$

where  $\Delta\sigma_{\perp}$  and  $\Delta\sigma_{\parallel}$  are the space-charge-induced shifts of betatron and synchrotron phase advances from the design values  $(\sigma_{\perp}, \sigma_{\parallel})$ . These shifts  $(\Delta\sigma_{\perp}, \Delta\sigma_{\parallel})$  are particle-dependent and thus unobservable. As repeatedly emphasized in our previous works (see, for example, Ref. [16]

together with Ref. [17]), the incoherent mechanism is effective only in the beam tail, where  $\Delta\sigma_{\perp}$  and/or  $\Delta\sigma_{\parallel}$  are relatively small. Equation (3) is generally useless in describing the stability of core particles that have large tune shifts in the three directions.

We must avoid incoherent tail resonance regions as well as low-order coherent core resonance bands to minimize the possibility of undesired particle losses. In circular machines, the incoherent resonance mechanism is probably of higher importance from a practical point of view. Since the tune depression is always close to unity in any synchrotrons and storage rings, nonlinear coherent instabilities in the beam core are not only weak but also spontaneously damped before causing a detectable level of beam loss [21,22]. In many cases, therefore, the incoherent mechanism should be responsible for particle losses observed in rings. It is, however, reasonable to avoid all low-order coherent resonance bands for safety to ensure the best beam quality. The coherent effect can be more influential in linear machines, but it never means that space-charge-induced resonances in linacs are essentially different from those in rings. A large discrepancy in typical beam density just changes a dominant instability mechanism that leads to major beam loss.

A couple of beam stability maps based on the semi-empirical resonance condition in Eq. (2) is depicted in Fig. 3 for reference. Coherent resonance bands of up to the third order (gray-shaded area) have been taken into consideration. According to our past experience with S-POD experiments, it is necessary to care about core resonances of the second and third orders at least. Most of these low-order stop bands (and/or tail resonances adjacent to them) are observable as demonstrated in later sections. Provided that a very high-density beam must be stored for a very long period, it is advisable to pay attention to fourth-order stop bands as well. In fact, we have detected a possible signature of fourth-order core instability in the case of long-term ion storage [20].

The widths of the stop bands in Fig. 3 are estimated from the simple formula given in Ref. [21]. The number of ions contained in the bunch is fixed all over the diagrams at the value that makes the transverse tune depression at  $(\sigma_{\perp}, \sigma_{\parallel}) = (48.1^{\circ}, 25.6^{\circ})$  equal to 0.95 in the upper panel and to 0.80 in the lower panel. The same operating point was used in the experiment to produce ion clouds in the LPT (see Sec. V). We have assumed the ion bunch to be in the equipartitioned state there [29]; the condition

$$\frac{\varepsilon_{\parallel}}{\varepsilon_{\perp}} = \frac{\eta_{\perp}\sigma_{\perp}}{\eta_{\parallel}\sigma_{\parallel}} \quad (4)$$

has been imposed at the ionization point.

The hatched areas in Fig. 3, where incoherent resonances may take place in the beam tail under the condition in Eq. (3), play a particularly important role in rings as

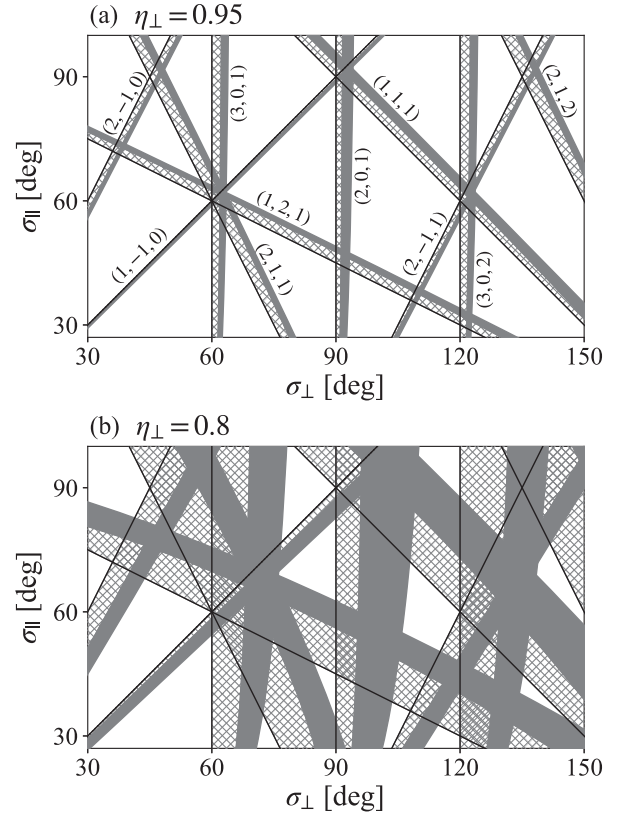


FIG. 3. Examples of stop-band diagrams (a) in the low-density regime and (b) in the high-density regime. In both cases, the bunch intensity and rms emittances have been fixed in the whole tune space. The transverse rms tune depression at the operating point  $(\sigma_{\perp}, \sigma_{\parallel}) = (48.1^{\circ}, 25.6^{\circ})$  has been adjusted to  $\eta_{\perp} = 0.95$  in the upper panel and to  $\eta_{\perp} = 0.80$  in the lower. Coherent core resonances of the second and third orders are expected to occur within gray shaded areas, provided  $C_2 = 0.7$  and  $C_3 = 0.8$ . Three integers written beside each band represent  $(n_{\perp}, n_{\parallel}, n)$  in Eq. (2). Incoherent resonances of tail particles can be excited within hatched areas. Pure synchrotron resonances with  $n_{\perp} = 0$  have been ignored here because of the reason discussed in Sec. IV.

explained above, but even in linacs, should be avoided. Note that the third-order difference resonance with  $(n_{\perp}, n_{\parallel}, n) = (1, -2, 0)$  is missing; under the initial emittance condition adopted here, this resonance is strongly suppressed according to one of the findings in Ref. [24]. Figure 3 predicts the existence of many betatron and synchrobetatron resonance bands, most of which were actually observed in the previous S-POD experiment using a static potential well in the axial direction [9]. A question is whether the periodic modulation of the axial focusing force adds any new feature beyond this theoretical expectation. This is certainly an important issue relevant to the basic design of any linac. Not only numerical but also convincing experimental evidence is needed to give a definitive answer to the question.

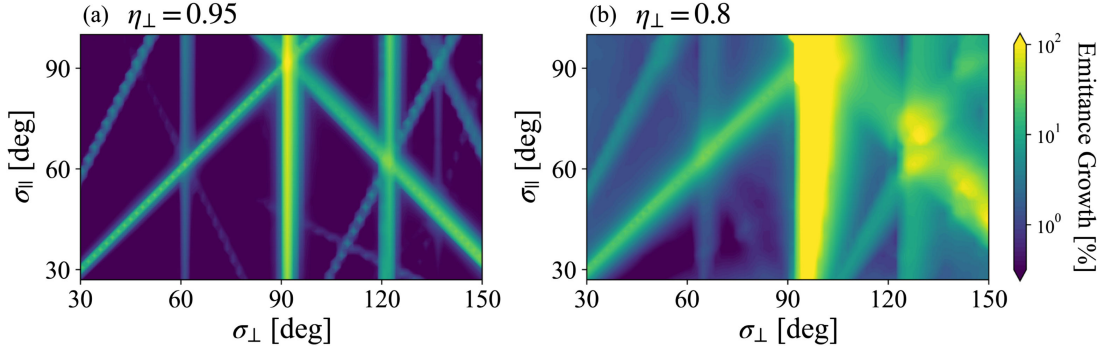


FIG. 4. PIC simulation results. The initial beam conditions are the same as assumed in Fig. 3. The highest emittance growth of the three directions is used to choose the color at each operating point.

#### IV. NUMERICAL SIMULATION RESULTS

Numerical simulations on 3D space-charge effects, even with the help of modern high-performance computers, are far more time-consuming than *experimental* simulations with the S-POD. It is, however, still informative to see what self-consistent simulation codes predict, even if we can only consider a short transport distance. The PIC code WARP was employed to simulate the dynamic behavior of an intense beam governed by the Hamiltonian in Eq. (1) [30]. In addition to the dominant linear potentials for transverse and axial ion confinements, a weak sextupole error field unavoidable in practice was introduced that somewhat enhances third-order resonances. The amplitude of this external nonlinear component is determined with a Poisson solver, assuming random electrode misalignments of 50  $\mu\text{m}$  on rms average. The transport distance is limited to 200 AG cells to save computational time.

We need to match the initial distribution of particles in phase space very carefully to the external AG lattice, including the effect of the strong Coulomb self-field potential. Ideally, the distribution must be in an equilibrium state reflecting a stationary solution to the Vlasov equation. Such fine-grained matching is essential to identify weak instabilities. If the initial matching is poor, a high-density beam will suffer non-negligible emittance growth everywhere right after injection, which obscures weak signatures of nonlinear resonances. We here start each PIC simulation with a pseudoequilibrium Gaussian distribution, employing the technique originally developed by Lund *et al.* [24,31].

Emittance growth rates numerically evaluated at about 3000 different operating points are color coded in Fig. 4. All the stop bands predicted in Fig. 3 by the coherent resonance theory can be seen though some of them are weak. As expected, no pure synchrotron resonance with  $n_{\perp} = 0$  is excited. Assuming a uniform bunch well-matched to an external quadrupole focusing lattice, we realize that the longitudinal space-charge force is insensitive to the transverse envelope oscillation driven by the AG lattice (see, for example, Ref. [11]). The actual period of the

longitudinal driving force is then a half of the transverse FODO period. We can readily verify, by solving the 3D envelope equations, that a matched beam executes almost identical oscillation twice axially within a single transverse AG cell [24]. Furthermore, the amplitude of the axial envelope modulation is very small because the beam receives not AG but weak focusing force in that direction. These facts suggest that only weak synchrotron resonances of the fourth order or higher can be excited in the range of  $\sigma_{\parallel}$  surveyed in Fig. 4. It should, however, be remembered that various error fields and noise sources are inevitable in real machines. Such imperfections affect the design periodicity of the focusing lattice, which might enhance the potential danger of low-order resonances especially above the line  $\sigma_{\parallel} = 90^{\circ}$ . A piece of information associated with this issue is offered in the Appendix for reference.

The growth rate of each resonance depends on the emittance condition of the incident beam. For instance, if the transverse and longitudinal emittances are equalized at the beginning, the difference resonance line with  $(n_{\perp}, n_{\parallel}, n) = (1, -1, 0)$  disappears [24]. As mentioned in the last section, the third-order difference resonance with  $(n_{\perp}, n_{\parallel}, n) = (1, -2, 0)$  is invisible here. This is because the equipartitioning condition in Eq. (4) has been imposed at  $(\sigma_{\perp}, \sigma_{\parallel}) = (48.1^{\circ}, 25.6^{\circ})$  when we determine the initial rms emittances. As the transverse tune is roughly twice greater than the longitudinal value, the emittance ratio  $\varepsilon_{\parallel}/\varepsilon_{\perp}$  of the equipartitioned beam is close to two. Then, the resonance band with  $(n_{\perp}, n_{\parallel}, n) = (1, -2, 0)$  is strongly suppressed according to the theory in Ref. [24].

Phase-space matching in a real machine is not as precise as numerically achieved here. Any beams probably have a significant amount of tail particles at injection, which will enhance emittance growth and resultant beam loss in the tail resonance regions, i.e., the hatched areas in the stability maps of Fig. 3. We also wish to point out the fact that the incoherent tune spread of a Gaussian core is quite large at the tune depression of 0.8; specifically, it exceeds  $30^{\circ}$  when  $\sigma_{\perp}$  or  $\sigma_{\parallel}$  goes beyond  $90^{\circ}$  per FODO cell. It thus seems

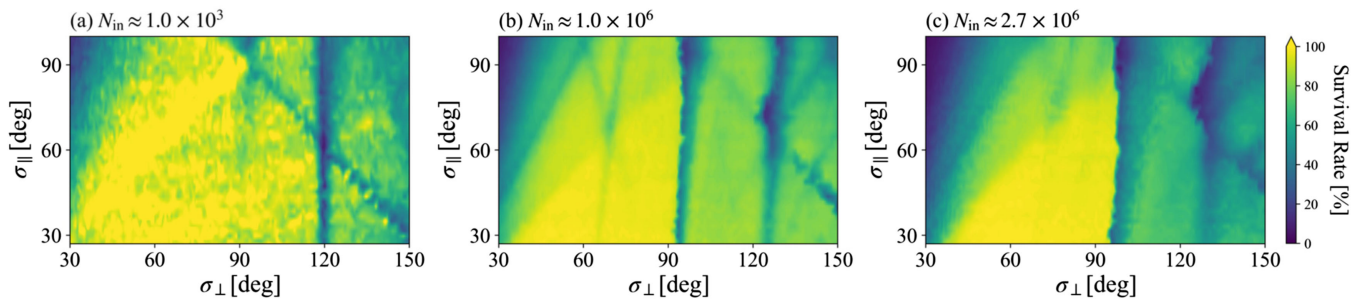


FIG. 5. Short-term stability maps experimentally obtained with the S-POD system. The period of ion storage is fixed at 0.5 ms (500 AG cells). The number of  $\text{Ar}^+$  ions initially stored in the LPT is about (a)  $1.0 \times 10^3$ , (b)  $1.0 \times 10^6$ , and (c)  $2.7 \times 10^6$ .

impossible for the necktie diagram to provide a rational explanation to the simulation data in Fig. 4.

## V. EXPERIMENTAL RESULTS

In contrast to 3D multiparticle simulations, we only need 5 s or so in the S-POD experiment to complete a single cycle of stability measurement at every operating point even for extremely long-term ion storage over millions of AG periods. More than  $10^6$   $\text{Ar}^+$  ions can be stored in the LPT (Fig. 1) designed for short-bunch experiments. The rms tune depression then reaches around 0.8 [32]. Following the earlier work [9], we first checked the best operating point at which the number of confineable ions is maximized. The result was almost identical to the previous one (see Fig. 3 of Ref. [9]). In the present experiment, we decided to use the operating point  $(\sigma_{\perp}, \sigma_{\parallel}) = (48.1^{\circ}, 25.6^{\circ})$  for ionization. Since we prepare an ion cloud spending about 1 s (a million AG periods), the bunch is most likely in a sort of equilibrium state initially.

Another fact worthy of attention is that the ionization occurs almost everywhere inside the LPT aperture. The safety margin is, therefore, not so wide as in the case of ordinary accelerators, which makes the S-POD experiment more sensitive to transverse emittance growth. This is important in detecting weak signals from coherent core resonances because they spontaneously cease to develop as the bunch density is reduced by the emittance growth. Since most large-scale accelerators have a high safety margin, it is probably difficult to identify nonlinear core resonances from simple beam-loss measurement; careful phase-space probing (emittance measurement) will be indispensable to know what happens in the beam core.

After a specific number of  $\text{Ar}^+$  ions are accumulated at  $(\sigma_{\perp}, \sigma_{\parallel}) = (48.1^{\circ}, 25.6^{\circ})$ , the operating point is moved to a target location in tune space within 100  $\mu\text{s}$  and stay there for a specific period. We then eject the ion cloud from the LPT to count the number of surviving particles with the MCP detector, but before the ejection, the operating point must be returned to the original ionization spot. As remarked in Sec. II, the transverse focusing force has been somewhat weakened by the axial ion confinement

potential. Once the axial potential barrier on the detector side is removed for ion extraction, this transverse defocusing effect disappears, leading to a sudden increase of the transverse phase advance. The betatron motion may then become unstable due to overfocusing in the transverse directions and, as a result, some ions would be lost before arriving at the detector. No such extra ion losses are expected at  $(\sigma_{\perp}, \sigma_{\parallel}) = (48.1^{\circ}, 25.6^{\circ})$  because  $\sigma_{\parallel}$  is relatively low (and thus, the transverse defocusing force created by  $V_{\parallel}$  is not so strong).

A wide range of tune space was surveyed to uncover dangerous operating regions where serious beam loss may occur in linacs. The number of ions surviving after 0.5 ms was measured at about 2800 different operating points distributed uniformly over the ranges  $30^{\circ} \leq \sigma_{\perp} \leq 150^{\circ}$  and  $27^{\circ} \leq \sigma_{\parallel} \leq 100^{\circ}$ . The measurement results are compiled into color-coded stability maps in Fig. 5 that visualize the distribution of low-order instability bands at three different  $N_{\text{in}}$ 's (the number of ions initially stored in the LPT). The lifetime of an ion cloud is well above a second ( $10^6$  AG cells), which means that natural ion losses through collisions with other ions and residual gas atoms are negligible in such a short storage period of 0.5 ms.

At low intensity [Fig. 5(a)], there are two apparent instability bands, one of which corresponds to  $(n_{\perp}, n_{\parallel}, n) = (3, 0, 2)$  and the other to  $(1, 1, 1)$ . The former resonance is particularly severe because it has been enhanced by third-order error fields originating from misalignments of the LPT electrodes. The wide ion-loss region around the upper-left corner is largely due to a shrinkage of the LPT acceptance [9].

At higher intensity [Figs. 5(b) and 5(c)], most of the resonance stop bands foreseen in Fig. 3 have appeared. The rms tune depression at  $N_{\text{in}} \approx 2.7 \times 10^6$  should be near 0.8, considering past S-POD data of long-bunch experiments [32]. We recognize that all stop bands significantly shift in the tune space from the positions of single-particle resonance lines. Some of them are even curved just as the theory in Sec. III predicts. The existence of the third-order sum resonance with  $(n_{\perp}, n_{\parallel}, n) = (1, 2, 1)$  is still unclear, which is consistent with the PIC simulation data in Fig. 4.

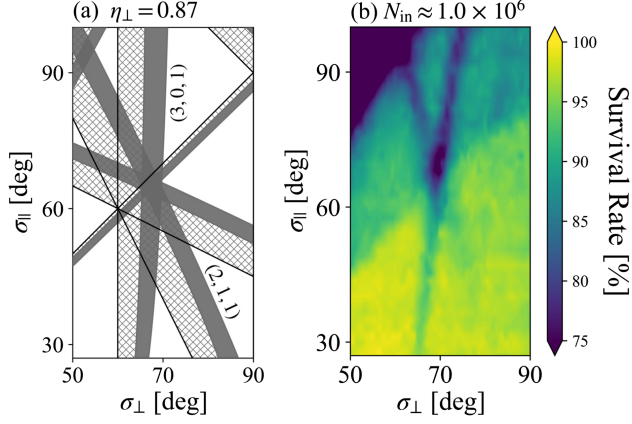


FIG. 6. Nonlinear stop bands in the range  $50^{\circ} < \sigma_{\perp} < 90^{\circ}$ . (a) Theoretically expected stop-band distribution corresponding to the experiment in the right panel. (b) Enlargement of Fig. 5(b) with a different color scale.

On the other hand, the stop band slightly above  $\sigma_{\perp} = 90^{\circ}$  has caused serious trouble in the high-density regime. The loss rate there is now higher than that on the third-order resonance with  $(n_{\perp}, n_{\parallel}, n) = (3, 0, 2)$  driven by both external error fields and the Coulomb self-field. This observation strongly suggests that the resonance near  $\sigma_{\perp} = 90^{\circ}$  is of the second order and driven mainly by the space-charge potential.

Since the operating point moves back and forth in tune space before the extraction of surviving ions, multiple resonance crossing occurs when we survey a high- $\sigma_{\perp}$  range above  $90^{\circ}$ . At least, one of the three low-order resonance bands with  $(n_{\perp}, n_{\parallel}, n) = (2, 0, 1)$ ,  $(3, 0, 2)$ , and  $(1, 1, 1)$  will be crossed twice, which results in extra ion losses even at an operating point free from resonance. The linear betatron resonance is most influential at high density. This is the reason for a slight reduction in the survival rate seen everywhere in the region  $\sigma_{\perp} \gtrsim 90^{\circ}$ .

A part of Fig. 5(b) is magnified in Fig. 6(b) with a different color scale to highlight ion losses due to nonlinear instability. The two stop bands crossing each other are clearly space-charge-induced because they become almost

invisible at low ion density as indicated in Fig. 5(a). The signature of the pure betatron resonance with  $(n_{\perp}, n_{\parallel}, n) = (3, 0, 1)$  has been repeatedly observed also in long-bunch experiments [12,13,18]. The conventional incoherent resonance condition as in Eq. (3) says that these resonances are highly nonlinear (of the sixth order), but then, we have trouble explaining why many other resonances of the sixth and lower orders are missing in the map. According to the resonance theory in Sec. III, both stop bands are of the third order (or due to accompanying incoherent losses of tail particles). The stability chart in Fig. 6(a) based on Eq. (2) looks in reasonable agreement with the experimental data. A slight discrepancy in the stop-band locations should probably come from an error in the theoretical estimate of the rms tune depressions; Figure 6(b) suggests that the bunch density in a high- $\sigma_{\parallel}$  range is a bit higher than our expectation.

We now extend the ion storage period from 0.5 to 10 ms corresponding to beam transport over  $10^4$  AG cells. The result is shown in Fig. 7, where three different values of  $N_{\text{in}}$  have been considered again. The extension of the storage period makes several weak nonlinear stop-bands observable. For instance, we newly discover a faint instability band between the two betatron resonances along  $\sigma_{\perp} \approx 60^{\circ}$  and  $90^{\circ}$ . That is believed to be caused by fifth-order error fields. Such weak, highly nonlinear resonances should, however, be much less dangerous than the low-order ones and thus of no serious effect in practice, unless the machine is extremely long or has strong error fields along the beam line.

## VI. CONCLUDING REMARKS

A detailed experimental study has been performed by means of the S-POD, a tabletop LPT-based apparatus, to reveal the collective nature of short hadron bunches traveling in an AG focusing channel. The unique experimental system allows us to make a wide-range survey in tune space and thus offers indisputable evidence for the existence of various resonance stop bands. In an earlier study, the longitudinal potential well was static. We here

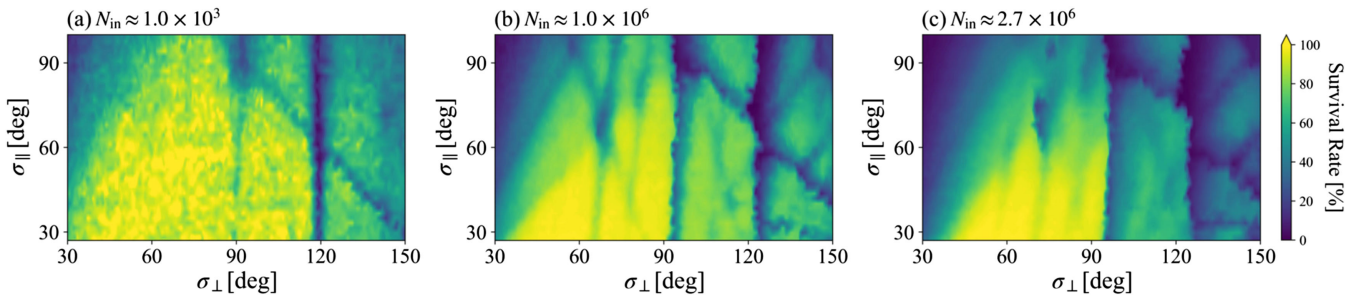


FIG. 7. Long-term stability maps experimentally obtained with the S-POD system. The period of ion storage is fixed at 10 ms (10,000 AG cells). The number of  $\text{Ar}^+$  ions initially stored in the LPT is about (a)  $1.0 \times 10^3$ , (b)  $1.0 \times 10^6$ , and (c)  $2.7 \times 10^6$ .

introduced a periodic modulation in the longitudinal ion focusing force to model a lattice condition in typical DTLs more precisely. It was found that this modification gives rise to no substantial change in the resonance feature elucidated by the previous study. Although the sinusoidal focusing potential was used instead of a discrete waveform, such simplification should have only little impact on the overall feature of resonance.

In the low-density regime where the space-charge effect is negligible, we can ensure the bunch stability over a wide tune range as long as the transport distance (ion storage period) is moderate. As illustrated in Fig. 5(a), no severe, low-order resonances appear below the lines  $\sigma_{\perp} = 120^{\circ}$  and  $\sigma_{\perp} + \sigma_{\parallel} = 180^{\circ}$  at least under the initial condition of an ion cloud in the LPT. The former is a third-order betatron resonance line enhanced by external error fields, while the latter is the synchrotron sum resonance of the lowest order.

At higher density, the coherent betatron resonance near  $\sigma_{\perp} = 90^{\circ}$ , the so-called *envelope instability* [1–3], becomes serious. In addition, several nonlinear betatron and synchrotron resonance stop bands manifest themselves below the phase advance of  $90^{\circ}$  per AG cell. These stop bands move and even bend in tune space, as expected from the resonance theory in Sec. III. Most ion losses observed in the high-density regime can be understood as a consequence of low-order coherent resonances in the core or accompanying incoherent tail resonances of twice the order. The new type of stability chart explains the experimental observations fairly well, which is supported by self-consistent numerical simulations. In contrast, the conventional necktie diagram relying on the concept of incoherent tune spread cannot provide a convincing explanation for the experimental and numerical results.

The S-POD data and theory presented in this paper should be useful not only in designing next-generation DTLs but also in improving the performance of operating hadron linacs. The new stability chart can be employed, for example, to optimize the operating condition of a high-intensity linac for emittance-growth minimization. If the operating point is kept out of possible dangerous areas predicted by the stop-band diagram, the beam will be basically stable throughout the acceleration process. Each stop-band indeed moves during acceleration, but the instability areas are generally the widest at the linac entrance. As the beam energy increases, the tune depressions at a specific operating point approach unity. All coherent resonance lines derived from Eq. (2) then shift toward their nearby single-particle resonance lines, while the widths of both coherent core and incoherent tail resonance domains get gradually narrower. In most cases, therefore, we simply have to pay attention to the initial stop-band distribution and control the energy-dependent

variation of the bare phase advances, such that the operating point stays in a resonance-free area until the linac exit.

We identified various synchrotron coupling resonance bands, but no noticeable synchrotron resonance with  $n_{\perp} = 0$  was observed unlike in the transverse degrees of freedom, where a few pure betatron resonances with  $n_{\parallel} = 0$  took place. The reason should be, in one word, the discrepancy in periodicity between the betatron and synchrotron motions; when the beam is well-matched to the external focusing potential, the synchrotron phase advance per actual oscillation period is not  $\sigma_{\parallel}$  defined conventionally for the FODO period but a half of  $\sigma_{\parallel}$ . The experimental observation is consistent with the multiparticle simulation results given in Sec. IV. Too large a synchrotron phase advance is, however, not strongly recommended for safety reasons. In fact, the natural acceptance and usable resonance-free parameter space tend to diminish as  $\sigma_{\perp}$  and/or  $\sigma_{\parallel}$  become greater. We must keep it in mind that the linac operating point generally moves as the beam is accelerated, so a sufficiently large resonance-free area is needed to avoid dangerous resonance crossing. We should also be careful about possible negative effects from beam mismatches and error fields unavoidable in actual accelerators. As suggested in the Appendix, the stability of the synchrotron motion can be affected seriously when the external beam focusing potential includes periodic error components.

## ACKNOWLEDGMENTS

This work is supported in part by JSPS KAKENHI (Grant No. 22K12671).

## APPENDIX: EXCITATION OF THE LONGITUDINAL ENVELOPE INSTABILITY

The absence of serious noncoupling synchrotron resonance ( $n_{\perp} = 0$ ) under the lattice condition in Fig. 2 has been well confirmed through self-consistent numerical simulations in Sec. IV and also in Ref. [24]. An interesting, practically important question is what happens if the ideal lattice symmetry assumed here is broken. The external electromagnetic forces acting upon a beam always include some errors in reality. Such machine imperfections may worsen the beam stability, strengthening original resonances, and even creating new stop bands. As an example, let us consider a case where the longitudinal rf field includes white noise; in particular, we here focus on the impact of the noise component whose wavelength is twice longer than the transverse AG period. This is probably one of the worst cases in terms of synchrotron resonance excitation.

Figure 8 shows PIC simulation data obtained with and without the longitudinal rf noise. In the right panel, a low



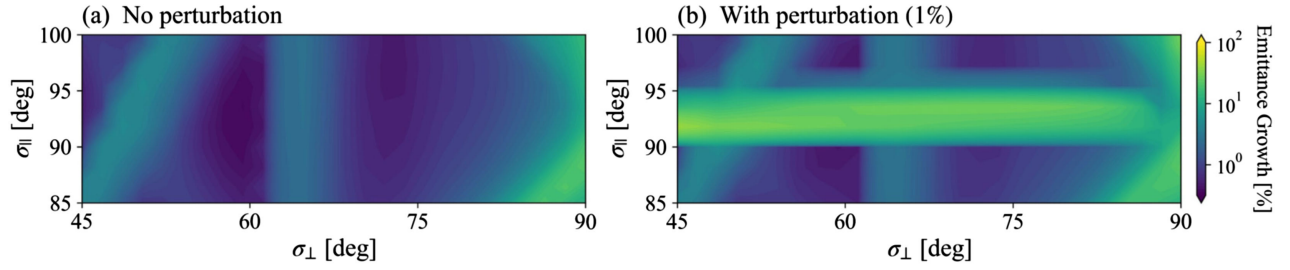


FIG. 8. PIC simulation results. (a) Emittance growth rates under the ideal rf focusing waveforms exhibited in Fig. 2. (b) Emittance growth rates evaluated with a perturbation wave (0.5 MHz) added to the axial focusing function  $K_{\parallel}(\tau)$ . The amplitude of the perturbation voltage is chosen 1% of the primary focusing wave of 2 MHz. The bunch intensity has been fixed at the value that gives  $\eta_{\perp} = 0.87$  at the ionization point.

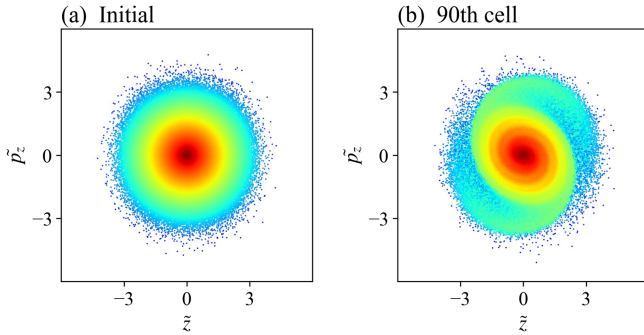


FIG. 9. Longitudinal phase-space configurations of the ion bunch at  $(\sigma_{\perp}, \sigma_{\parallel}) = (59.4^{\circ}, 93.6^{\circ})$  in Fig. 8(b). (a) The distribution of ions at the entrance. (b) The distribution of ions at the 90th AG cell. The abscissa and ordinate are the longitudinal canonical variables scaled with their rms values at the entrance.

rf voltage is added to the two quadrupole sections on both sides of the central section (see Fig. 1). The longitudinal focusing function  $K_{\parallel}$  is now the sum of the major cosine wave depicted in Fig. 2 and an additional perturbing rf wave of 0.5 MHz. The amplitude of the perturbation is adjusted to 1% of the main focusing wave of 2 MHz. A clear instability band has been formed above  $\sigma_{\parallel} = 90^{\circ}$  in Fig. 8(b) due to a pure synchrotron resonance. A relatively

high growth rate, compared with the other visible stop bands ( $m = 3$ ), implies that this axial instability is likely of the second order ( $m = 2$ ). In fact, the phase-space configuration in Fig. 9 has indicated the excitation of second-order resonance in the longitudinal direction.

The experimental confirmation of noncoupling synchrotron resonance is a bit tricky because we have no emittance monitor available at present. Unlike in the transverse directions where four electrode rods are sitting only 5 mm away from the LPT axis, there are no obstacles in the longitudinal direction to remove weakly unstable ions. An unambiguous signature of pure synchrotron resonance is observable only when a sufficient number of ions go beyond the potential barrier provided by  $V_{\parallel}$ . In this sense, the perturbation amplitude used for the PIC simulation in Fig. 8(b) is too small as we see from the resultant low emittance growth (less than 30% in 200 cells). In the experiment, therefore, we tried a much higher voltage (20% of the primary focusing-wave amplitude) to excite the synchrotron resonance strongly. Figure 10 shows the result of a stability survey with the S-POD, revealing the presence of the synchrotron resonance just above  $\sigma_{\parallel}$  of  $90^{\circ}$ . The numerical and experimental observations here suggest that the use of a high  $\sigma_{\parallel}$  over  $90^{\circ}$  is risky in practice.

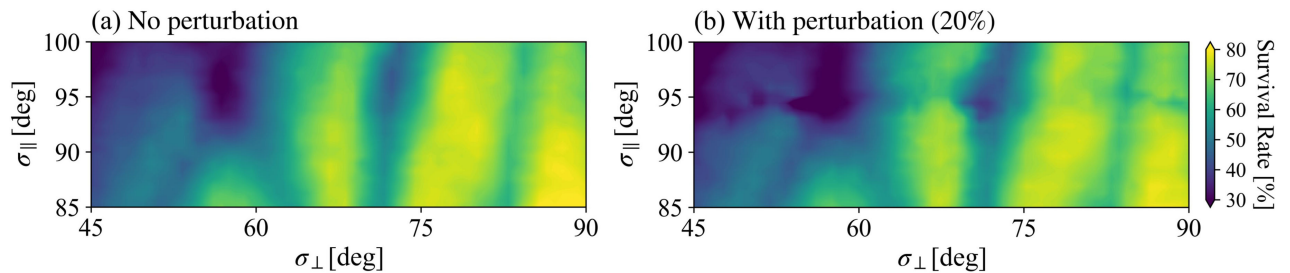


FIG. 10. Stability map obtained with the S-POD at  $N_{\text{in}} \approx 1.0 \times 10^6$ . The ion storage period is fixed at 10 ms. (a) Ideal case: reproduction of Fig. 7(b) for comparison. (b) Example with a longitudinal imperfection potential: the rf perturbation as considered in Fig. 8(b) is added to  $V_{\parallel}$ . The frequency of this additional field is the same as in the case of Fig. 8(b), but its amplitude has been set 20 times larger to enhance ion losses in the axial direction.

- [1] M. Reiser, *Theory and Design of Charged Particle Beams* (John Wiley & Sons, New York, 2008) and references therein.
- [2] I. Hofmann, L. J. Laslett, L. Smith, and I. Haber, Stability of the Kapchinskij-Vladimirskij (K-V) distribution in long periodic transport systems, Part. Accel. **13**, 145 (1983).
- [3] J. Struckmeier, J. Klabunde, and M. Reiser, On the stability and emittance growth of different particle distributions in a long magnetic quadrupole channel, Part. Accel. **15**, 47 (1984).
- [4] R. Takai, H. Enokizono, K. Ito, Y. Mizuno, K. Okabe, and H. Okamoto, Development of a compact plasma trap for experimental beam physics, *Jpn. J. Appl. Phys.* **45**, 5332 (2006).
- [5] S. L. Sheehy, E. J. Carr, L. K. Martin, K. Budzik, D. J. Kelliher, S. Machida, and C. R. Prior, Commissioning and first results of the Intense Beam EXperiment (IBEX) linear Paul trap, *J. Phys. Conf. Ser.* **874**, 012067 (2017).
- [6] H. Okamoto and H. Tanaka, Proposed experiment for the study of beam halo formation, *Nucl. Instrum. Methods Phys. Res., Sect. A* **437**, 178 (1999).
- [7] H. Okamoto, Y. Wada, and R. Takai, Radio-frequency quadrupole trap as a tool for experimental beam physics, *Nucl. Instrum. Methods Phys. Res., Sect. A* **485**, 244 (2002).
- [8] H. Okamoto, K. Kojima, and K. Ito, A compact Paul ion trap for the study of space-charge effects in drift-tube linear accelerators, *Prog. Theor. Exp. Phys.* **2019**, 093G01 (2019).
- [9] M. Goto, C. Ichikawa, K. Ito, K. Kojima, and H. Okamoto, Stability study of intense hadron bunches in linear accelerators using a Paul ion trap, *Phys. Rev. Accel. Beams* **25**, 054201 (2022).
- [10] P. K. Ghosh, *Ion Traps* (Oxford Science, Oxford, 1995).
- [11] T. P. Wangler, *RF Linear Accelerators* (John Wiley & Sons, New York, 1998).
- [12] K. Fukushima, K. Ito, H. Okamoto, S. Yamaguchi, K. Moriya, H. Higaki, T. Okano, and S. M. Lund, Experimental verification of resonance instability bands in quadrupole doublet focusing channels, *Nucl. Instrum. Methods Phys. Res., Sect. A* **733**, 18 (2014).
- [13] K. Ito, H. Okamoto, Y. Tokashiki, and K. Fukushima, Coherent resonance stop bands in alternating gradient beam transport, *Phys. Rev. Accel. Beams* **20**, 064201 (2017).
- [14] L. Smith, Effect of gradient errors in the presence of space charge forces, in *Proceedings of the 4th International Conference on High-Energy Accelerators, HEACC 1963, Dubna, Russian Federation* (Literary Licensing, LLC, 1963), p. 1232, <https://inspirehep.net/files/d370609bdc08510e69d7ed21c3b754ae>.
- [15] R. Baartman, Betatron resonances with space charge, *AIP Conf. Proc.* **448**, 56 (1998).
- [16] K. Kojima, H. Okamoto, and Y. Tokashiki, Empirical condition of betatron resonances with space charge, *Phys. Rev. Accel. Beams* **22**, 074201 (2019).
- [17] K. Kojima, H. Okamoto, and Y. Tokashiki, Reply to “Comment on ‘Empirical condition of betatron resonances with space charge’”, *Phys. Rev. Accel. Beams* **23**, 028002 (2020).
- [18] K. Moriya, M. Ota, K. Fukushima, M. Yamaguchi, K. Ito, and H. Okamoto, Double stop-band structure near half-integer tunes in high-intensity rings, *Phys. Rev. Accel. Beams* **19**, 114201 (2016).
- [19] H. Okamoto, M. Endo, K. Fukushima, H. Higaki, K. Ito, K. Moriya, S. Yamaguchi, and S. M. Lund, Experimental simulation of beam propagation over long path lengths using radio-frequency and magnetic traps, *Nucl. Instrum. Methods Phys. Res., Sect. A* **733**, 119 (2014).
- [20] T. Ikeda, K. Ito, and H. Okamoto, Novel tabletop experiment demonstrating the nonlinear resonance excitation observed at the CERN Proton Synchrotron, *Jpn. J. Appl. Phys.* **60**, 070901 (2021).
- [21] H. Okamoto, M. Aoki, C. Ichikawa, K. Kojima, T. Kurauchi, and Y. Yamane, Coherent and incoherent space-charge effects in high-intensity hadron rings, *J. Instrum.* **15**, P07017 (2020).
- [22] K. Kojima and H. Okamoto, Characterization of overlapping betatron resonances above the phase advance of 90° per cell, *Phys. Rev. Accel. Beams* **25**, 024201 (2022).
- [23] H. Okamoto and K. Yokoya, Parametric resonances in intense one-dimensional beams propagating through a periodic focusing channel, *Nucl. Instrum. Methods Phys. Res., Sect. A* **482**, 51 (2002).
- [24] Y. Yamane, H. Okamoto, and K. Kojima, Excitation and suppression of synchrobetatron resonances in high-intensity hadron linacs, *Phys. Rev. Accel. Beams* **24**, 084201 (2021).
- [25] F. J. Sacherer, rms envelope equations with space charge, *IEEE Trans. Nucl. Sci.* **NS-18**, 1105 (1971).
- [26] F. J. Sacherer, Ph.D. thesis, Transverse space-charge effects in circular accelerators, Lawrence Radiation Laboratory, Report No. UCRL-18454, 1968.
- [27] L. K. Martin, S. Machida, D. J. Kelliher, and S. L. Sheehy, A study of coherent and incoherent resonances in high intensity beams using a linear Paul trap, *New J. Phys.* **21**, 053023 (2019).
- [28] S. Ohtsubo, M. Fujioka, H. Higaki, K. Ito, H. Okamoto, and H. Sugimoto, Experimental study of coherent betatron resonances with a Paul trap, *Phys. Rev. ST Accel. Beams* **13**, 044201 (2010).
- [29] R. A. Jameson, Beam-intensity limitations in linear accelerators, *IEEE Trans. Nucl. Sci.* **28**, 2408 (1981).
- [30] D. P. Grote, A. Friedman, G. Craig, I. Haber, and W. Sharp, Progress toward source-to-target simulation, *Nucl. Instrum. Methods Phys. Res., Sect. A* **464**, 563 (2001).
- [31] S. M. Lund, T. Kikuchi, and R. C. Davidson, Generation of initial kinetic distributions for simulation of long-pulse charged particle beams with high space-charge intensity, *Phys. Rev. ST Accel. Beams* **12**, 114801 (2009).
- [32] K. Ito, T. Kurauchi, H. Higaki, and H. Okamoto, Experimental observation of low-order collective oscillation modes in a strong-focusing lattice, *J. Phys. Conf. Ser.* **1350**, 012125 (2019).